Table S1. DNA substrates used in the current study.

Name	**Oligo sequence** (5′-3′)
	Substrates for single-molecule FRET
dT_{10}	GCGTGGCACCGGTAATAGGAAATAGGAGATTTTTTTTTT(Cy3)
dT_{20}	GCGTGGCACCGGTAATAGGAAATAGGAGATTTTTTTTTTTTTTTTTTT(Cy3)
dT_{30}	GCGTGGCACCGGTAATAGGAAATAGGAGATTTTTTTTTTTTTTTTTTTTTTTTTTTT(Cy3)
dT_{40}	GCGTGGCACCGGTAATAGGAAATAGGAGATTTTTTTTTTTTTTTTTTTTTTTTTTTTTTTTTTTTT(Cy3)
dT_{60}	GCGTGGCACCGGTAATAGGAAATAGGAGATTTTTTTTTTTTTTTTTTTTTTTTTTTTTTTTTTTTTTTTTTTTTTTT(Cy3)
Stem1	(Cy5)TCTCCTATTTCCTATTACCGGTGCCACGC-biotin
Stem2	TTTTTTTTTTTTTTTTTTTTTTTTTTTTTCTCCT(iCy5)ATTTCCTATTACCGGTGCCACGC-biotin
dT_{10}^{*}	(Cy3)TTTTTTTTTTATGTATGACAAGGAAGG
dT_{20}^{*}	(Cy3)TTTTTTTTTTTTTTTTTTTTATGTATGACAAGGAAGG
dT_{30}^{*}	(Cy3)TTTTTTTTTTTTTTTTTTTTTTTTTTTTTTTTATGTATGACAAGGAAGG
dT_{40}^{*}	(Cy3)TTTTTTTTTTTTTTTTTTTTTTTTTTTTTTTTTTTTTTTTTTTTATGTATGACAAGGAAGG
Stem3	Biotin-CCTTCCTTGTCATACAT(Cy5)
dU_{10}	CGUCGAGCAGAGAUUUUUUUUUU(Cy3)
dU_{20}	CGUCGAGCAGAGAUUUUAUUUUAUUUUAUUUUA(Cy3)
dU_{30}	CGUCGAGCAGAGAUUUUAUUUUAUUUUAUUUUAUUUUAUUUUA(Cy3)
Stem4	CTCT(iCy5)GCTCGACG-Biotin
	Substrate for equilibrium DNA-binding assay
s_{32}	CACTGGCCGTCTTACGGTCGCTCTGCTCGACG-FAM
	Substrates for gel filtration analysis
dT_{10}	GCGTGGCACCGGTAATAGGAAATAGGAGATTTTTTTTTT
dT_{20}	GCGTGGCACCGGTAATAGGAAATAGGAGATTTTTTTTTTTTTTTTTTT
dT_{30}	GCGTGGCACCGGTAATAGGAAATAGGAGATTTTTTTTTTTTTTTTTTTTTTTTTTTT
dT_{60}	GCGTGGCACCGGTAATAGGAAATAGGAGATTTTTTTTTTTTTTTTTTTTTTTTTTTTTTTTTTTTTTTTTTTTTTT
Stem	TCTCCTATTTCCTATTACCGGTGCCACGC

Internal Cy5 (iCy5) in oligo was modified by the N-hydroxysuccinimide (NHS) ester form of Cy5 in thymine with a 12-atom linker.

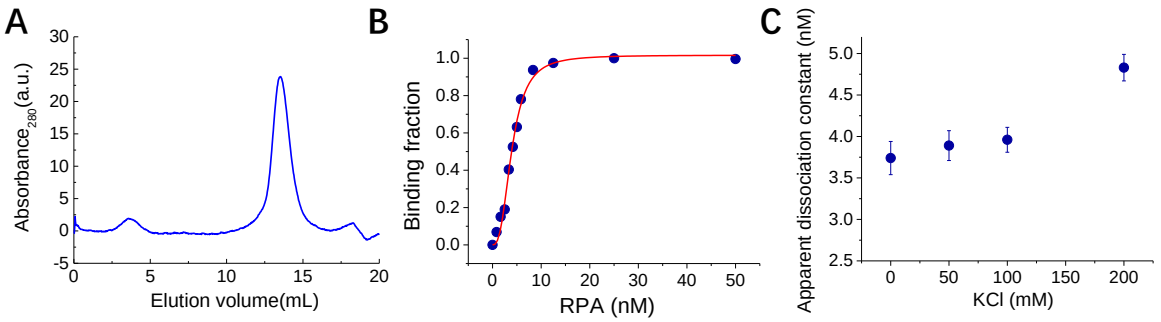

Figure S1. Binding of RPA to ssDNA in different buffers. (A) Gel filtration of RPA. The elution profile corresponds to the absorbance of 280 nm ultraviolet ray. (B) Binding fractions of RPA on a 32 nt ssDNA substrate in 100 mM KCl determined by fluorescence polarization assay. The binding curve was fitted by Hill equation $y = [RPA]^n / (K_D^n + [RPA]^n)$, where y is binding fraction, n is Hill coefficient, and K_D is the apparent dissociation constant. (C) The apparent dissociation constant K_D in different buffer conditions. Error bar denotes the standard deviation. The K_D value only increases slightly from 0 to 100 mM KCl; however, in 200 mM KCl, the binding becomes worse, possibly due to the increased electrostatic screening.

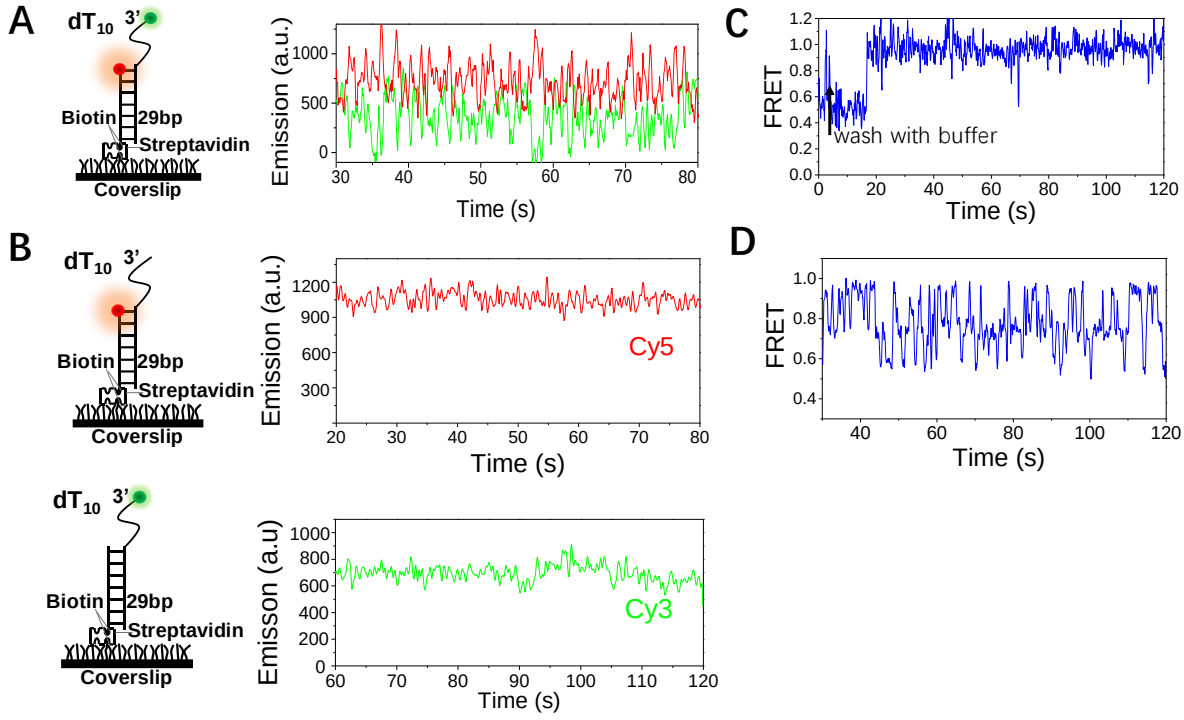

Figure S2. Binding of RPA to dT_{10}. (A) The original fluorescence traces of dT_{10} in 20 nM RPA shown in Figure 1D. (B) Addition of 20 nM RPA did not lead to the fluctuations of fluorescence signals if only one fluorophore (Cy5 or Cy3) was labeled on the DNA. (C) After association with 200 nM RPA, washing the fluidic cell with buffer results in the dissociation of the protein from dT_{10}. (D) Selected FRET traces of dT_{10} in the presence of 20 nM RPA. During the quick association and dissociation process, a subtle intermediate state can be occasionally observed.

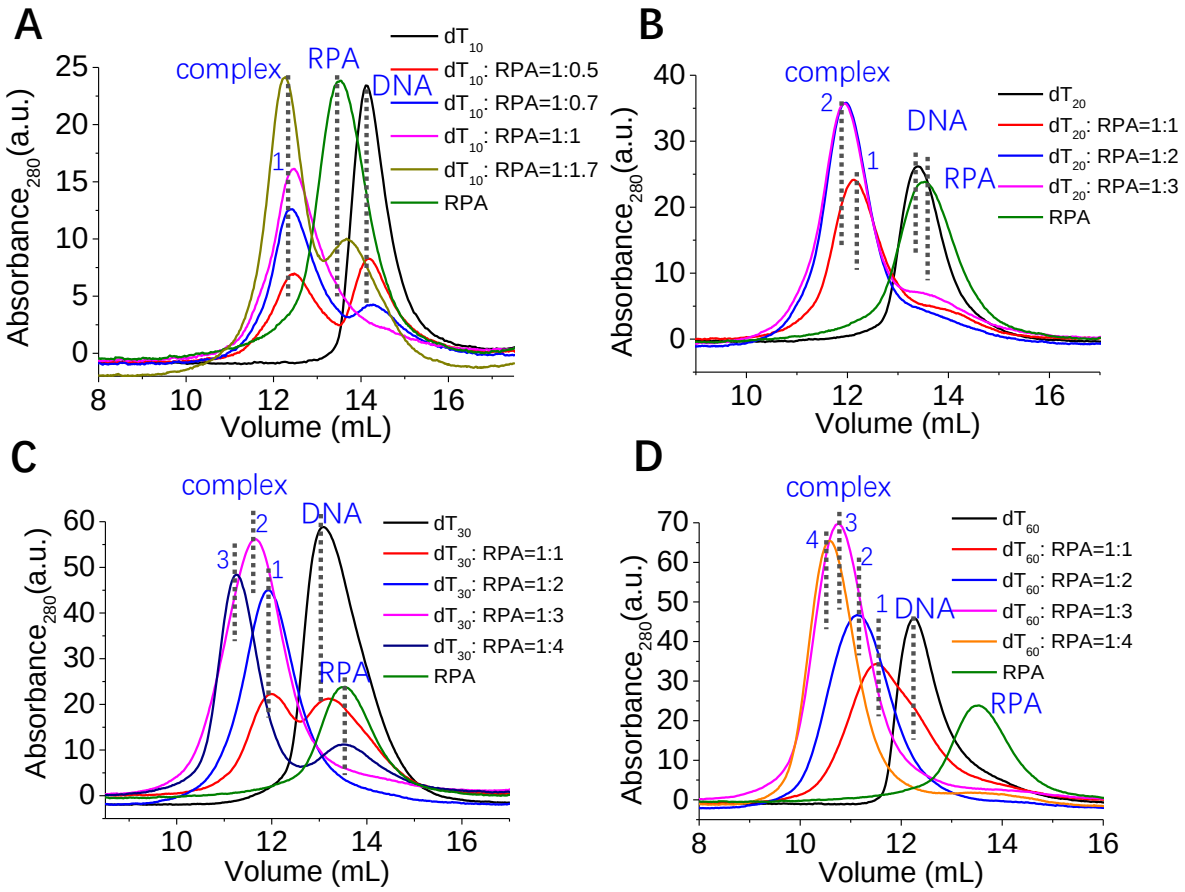

Figure S3. RPA forms different types of complexes with ssDNA. Gel filtration was performed as described in the 'Materials and Methods'. A.u. denotes arbitrary unit. It is worth noting that, the gel filtration results can be used to roughly estimate how many different types of DNA-protein complexes have been formed; however, the exact stoichiometry of DNA and protein in the complex cannot be precisely obtained. (A) RPA forms one type of complex with a 10 nt ssDNA in a wide range of protein concentrations. (B) RPA can form two different types of complexes with a 20 nt ssDNA in a wide range of protein concentrations. (C) RPA can form three different types of complexes with a 30 nt ssDNA in a wide range of protein concentrations. (D) RPA can form four different types of complexes with a 60 nt ssDNA in a wide range of protein concentrations without the excess of protein. It is likely that, with the further increasing of protein concentration, new types of complexes may be formed.

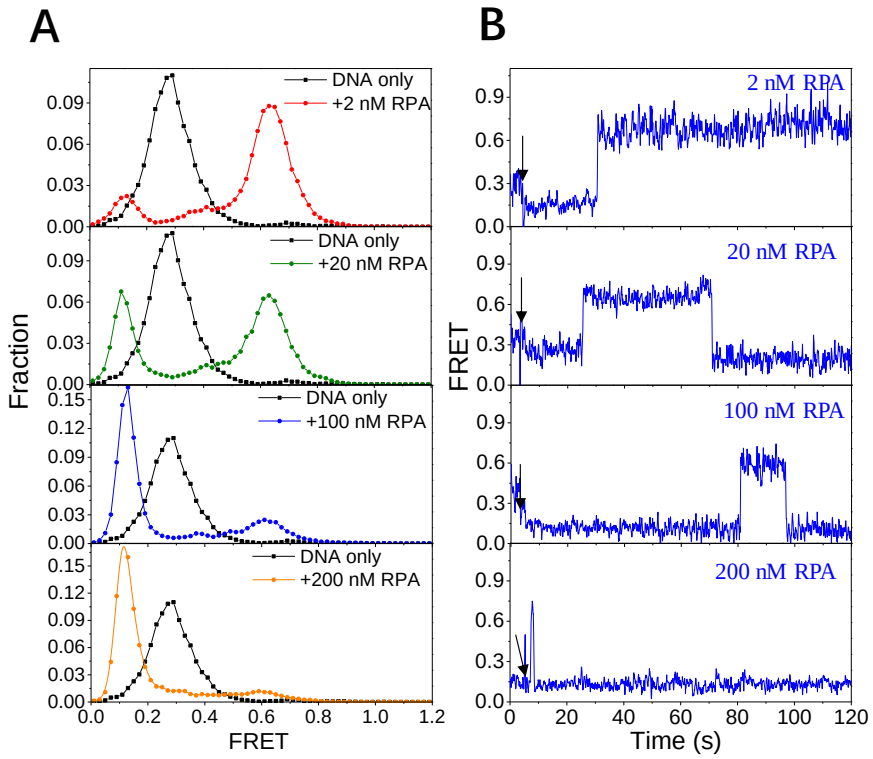

Figure S4. RPA induces the bending of a 40 nt ssDNA. (A) FRET histograms of DNA substrate dT_{40} alone and in the presence of varied concentrations of RPA. Each FRET histogram was constructed from more than 300 traces. (B) Representative FRET traces for dT_{40} in different concentrations of RPA. Black arrows indicate the addition of RPA.

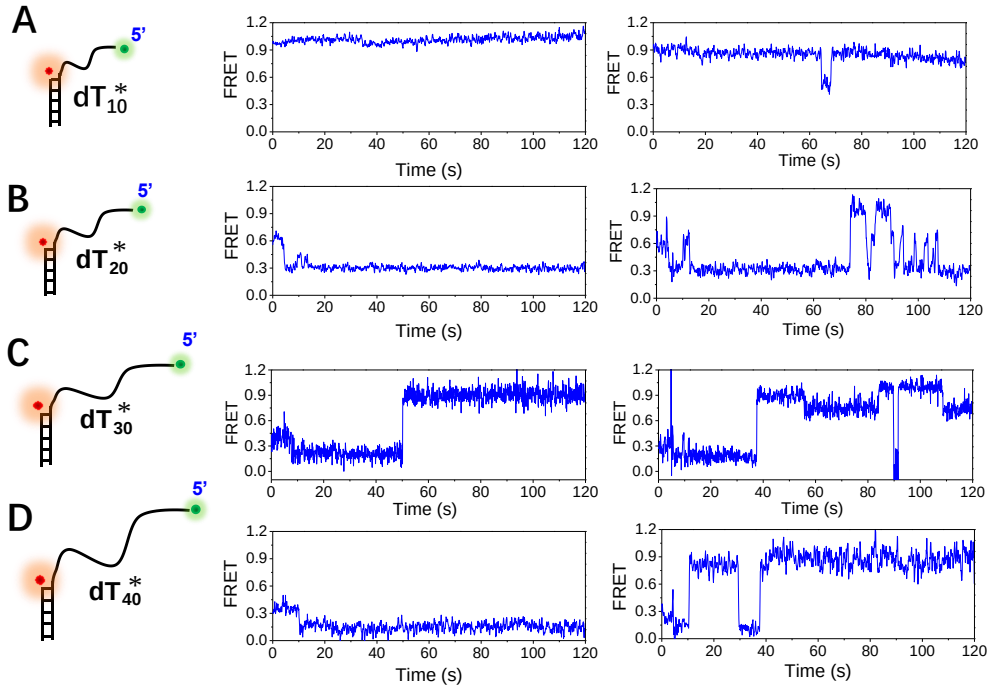

Figure S5. Representative FRET traces for ssDNA at the 5′ end of the duplex in the presence of 2 nM RPA. (A) RPA seldomly binds to dT_{10}^{*}. (B) The association of RPA can lead to both the decrease and increase of the FRET efficiency in dT_{20}^{*}. (C) The association of RPA can lead to both the decrease and increase of the FRET efficiency in dT_{30}^{*}. (D) The association of RPA can lead to both the decrease and increase of the FRET efficiency in dT_{40}^{*}.

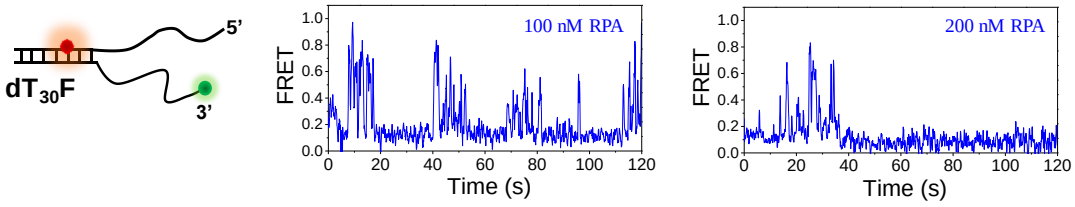

Figure S6. Selected FRET traces of $dT_{30}F$ in the presence of 100-200 nM RPA. Very quick bursts of FRET value can be observed, similarly as that in 2-20 nM RPA in Figure 6D.

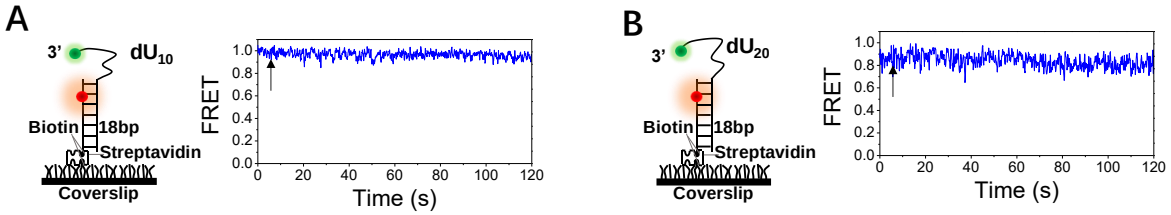

Figure S7. RPA cannot bind to dU_{10} (A) and dU_{20} (B).

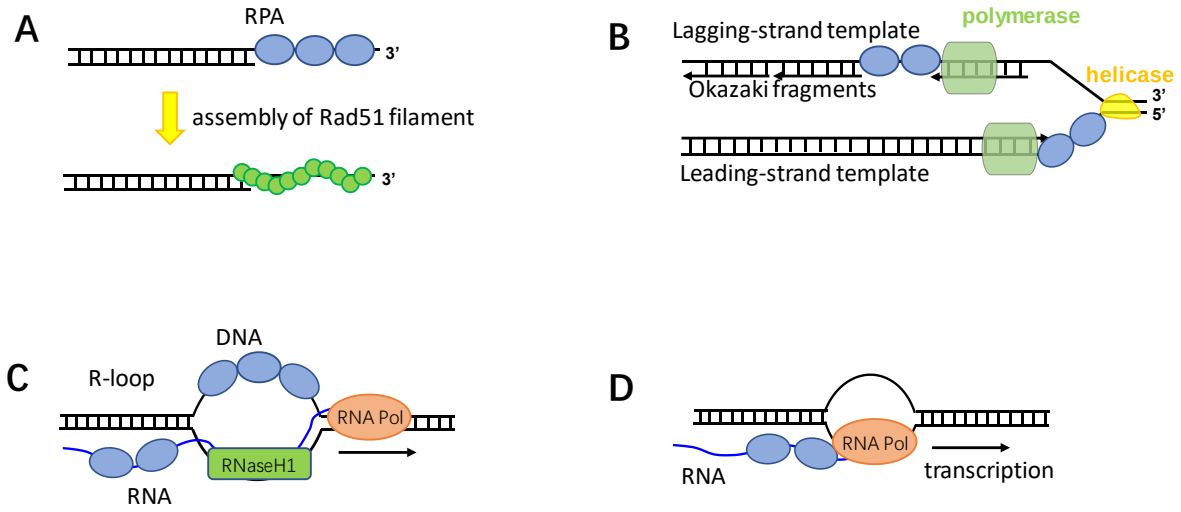

Figure S8. Potential cellular functions of the dynamic RPA binding with single-stranded DNA or RNA in different DNA processing pathways. (A) The early stage of homologous recombination; (B) The stalled replication fork generated by the uncoupling of helicase and the polymerase, or the synthesis of Okazaki fragment in the lagging strand DNA replication; (C) R-loops generated in DNA transcription; (D) RPA localizes to the transcribed regions of active genes, and correlates with the RNA Pol.